SANDIA REPORT
SAND2010-7217
Unlimited Release
Printed November 2010

Natural Materials for Carbon Capture

Randall T. Cygan, Vyacheslav N. Romanov, and Evgeniy M. Myshakin

Prepared by
Sandia National Laboratories
Albuquerque, New Mexico 87185 and Livermore, California 94550

Sandia National Laboratories is a multi-program laboratory managed and operated by Sandia Corporation, a wholly owned subsidiary of Lockheed Martin Corporation, for the U.S. Department of Energy's National Nuclear Security Administration under contract DE-AC04-94AL85000.

Approved for public release; further dissemination unlimited.

Issued by Sandia National Laboratories, operated for the United States Department of Energy by Sandia Corporation.

NOTICE: This report was prepared as an account of work sponsored by an agency of the United States Government. Neither the United States Government, nor any agency thereof, nor any of their employees, nor any of their contractors, subcontractors, or their employees, make any warranty, express or implied, or assume any legal liability or responsibility for the accuracy, completeness, or usefulness of any information, apparatus, product, or process disclosed, or represent that its use would not infringe privately owned rights. Reference herein to any specific commercial product, process, or service by trade name, trademark, manufacturer, or otherwise, does not necessarily constitute or imply its endorsement, recommendation, or favoring by the United States Government, any agency thereof, or any of their contractors or subcontractors. The views and opinions expressed herein do not necessarily state or reflect those of the United States Government, any agency thereof, or any of their contractors.

Printed in the United States of America. This report has been reproduced directly from the best available copy.

Available to DOE and DOE contractors from
U.S. Department of Energy
Office of Scientific and Technical Information
P.O. Box 62
Oak Ridge, TN 37831

Telephone: (865) 576-8401
Facsimile: (865) 576-5728
E-Mail: reports@adonis.osti.gov
Online ordering: http://www.osti.gov/bridge

Available to the public from
U.S. Department of Commerce
National Technical Information Service
5285 Port Royal Rd.
Springfield, VA 22161

Telephone: (800) 553-6847
Facsimile: (703) 605-6900
E-Mail: orders@ntis.fedworld.gov
Online order: http://www.ntis.gov/help/ordermethods.asp?loc=7-4-0#online

SAND2010-7217
Unlimited Release
Printed November 2010

Natural Materials for Carbon Capture

Randall T. Cygan
Geochemistry Department
Sandia National Laboratories
P.O. Box 5800
Albuquerque, New Mexico 87185-0754

Vyacheslav N. Romanov
Geosciences Division
National Energy Technology Laboratory
P.O. Box 10940
Pittsburgh, Pennsylvania 15236

and

Evgeniy M. Myshakin
URS, National Energy Technology Laboratory
P.O. Box 10940
Pittsburgh, Pennsylvania 15236

Abstract

Naturally occurring clay minerals provide a distinctive material for carbon capture and carbon dioxide sequestration. Swelling clay minerals, such as the smectite variety, possess an aluminosilicate structure that is controlled by low-charge layers that readily expand to accommodate water molecules and, potentially, carbon dioxide. Recent experimental studies have demonstrated the efficacy of intercalating carbon dioxide in the interlayer of layered clays but little is known about the molecular mechanisms of the process and the extent of carbon capture as a function of clay charge and structure. A series of molecular dynamics simulations and vibrational analyses have been completed to assess the molecular interactions associated with incorporation of CO_2 in the interlayer of montmorillonite clay and to help validate the models with experimental observation.

ACKNOWLEDGMENTS

This work was funded in part by the Sandia National Laboratories Laboratory Directed Research and Development Program. The authors are appreciative of the support of John Merson and Mark Rigali at Sandia National Laboratories and George Guthrie at National Energy Technology Laboratory to help expand fundamental research on carbon capture using clay materials. Additional support was provided by the Center for Frontiers of Subsurface Energy Security, an Energy Frontier Research Center funded by the U.S. Department of Energy, Office of Science, Office of Basic Energy Sciences under Award Number DE-SC-0001114. Sandia National Laboratories is a multi-program laboratory operated by Sandia Corporation, a wholly owned subsidiary of Lockheed Martin Corporation, for the U.S. Department of Energy's National Nuclear Security Administration under Contract DE-AC04–94AL85000.

CONTENTS

1. Introduction 7

2. Molecular Simulations 9
   2.1. Molecular Models of Montmorillonite 9
   2.2. Computational Methods 11
      2.2.1. Classical Methods 11
      2.2.2. Quantum Methods 12

3. Results and Discussion 15
   3.1. Classical Simulations 15
      3.1.1. Development of CO_2 Force Field 15
      3.1.2. Molecular Dynamics Simulations 17
      3.1.3. Power Spectra 19
   3.2. Quantum Simulations 22

4. Conclusions 25

5. References 27

Distribution 31

FIGURES

Figure 1. Adsorption of CO_2 in coal and various clay materials; montmorillonite (STx) and kaolinite (KGa) samples exhibit limited adsorption at low pressures but swell at supercritical conditions above 10 MPa. 8

Figure 2. Structure of 2 x 1 x 2 Na-montmorillonite cell exhibiting two layers of the aluminosilicate lattice; Mg atoms (blue) substitute for Al (pink) in the octahedral sheet; interlayer Na cations are represented as green spheres. 9

Figure 3. Snapshot of an equilibrated molecular dynamics simulation of sodium montmorillonite showing the Na^+ and water molecules in the interlayer; projection view is along the *b*-axis. 10

Figure 4. Swelling behavior of a montmorillonite clay based on *NPT* molecular dynamics simulations. 11

Figure 5. Simulation cells for molecular dynamics simulations of CO_2 as gas with 1408 molecules (left) and liquid with 512 molecules (right). Both simulations were equilibrated at 300 K and 5.6 MPa. 18

Figure 6. Equilibrated supercell structure of CO_2-montmorillonite model from molecular dynamics simulation using *NPT* ensemble at 310 K and 0.02 GPa. Projection view is along *b*-axis. 18

Figure 7. Power spectra for gas and liquid forms of CO_2 at 300 K and 5.6 MPa. 19

Figure 8. Power spectrum for the CO_2-montmorillonite derived from analysis of all atoms in the molecular dynamics trajectory. 20

Figure 9. Power spectra for the CO_2 atoms in liquid CO_2 and interlayer CO_2 from the intercalated montmorillonite derived from analysis of the molecular dynamics trajectories. 21

Figure 10. Detail of the CO_2 bend mode in the power spectra for the CO_2 atoms in liquid CO_2 and interlayer CO_2 from the intercalated montmorillonite. 22

TABLES

Table 1. Force Field Parameters for CO_2 17

Table 2. Normal Mode Analysis of Quantum-Derived CO_2 Cluster Models 23

1. INTRODUCTION

Naturally occurring clay minerals provide a distinctive material for carbon capture and carbon dioxide sequestration. In particular, swelling clay minerals, such as the smectite variety, possess an aluminosilicate structure that is controlled by low-charge layers that easily expand to accommodate water molecules and, potentially, carbon dioxide. The interlayer of smectite clays also includes counterbalancing cations such as sodium that balance the negative layer charge. Recent experimental studies have demonstrated the efficacy of intercalating CO_2 in the interlayer of layered clays (e.g.,Wang et al., 2003a) but little is known about the molecular mechanisms of the process and the extent of carbon capture as a function of clay charge and structure. In economic terms, clay minerals are a common natural resource and are literally dirt cheap. Clay minerals are an attractive alternative to more complex materials that often require significant chemical functionalization to ensure acceptable carbon capture performance (e.g., Favre et al., 2009; Bacsik et al., 2010; Zhao et al., 2010). Clay-based materials could have a distinct advantage in that they can be used once and buried, saving the cost of regenerative energy, CO_2 compression, and subsurface injection.

Sodium montmorillonite clay is a common clay mineral that has the potential for capture of CO_2, and provides a relatively stable environment for burial to help reduce carbon effects on the climate. The solubility of CO_2 within the interlayer of montmorillonite at both ambient conditions and at elevated conditions is unknown. It has been suggested that confinement of water modifies the dielectric constant of the water (Wang et al., 2003b), and can shift the acid constants of the confining surfaces and ultimately affect the solubility of CO_2. Experimental studies have been performed by Romanov and colleagues at the National Energy Technology Laboratory in Pittsburgh to confirm the insertion and retention of CO_2 in the interlayer of montmorillonite. Infrared spectroscopy at NETL has been used to monitor the conditions of insertion and the relative stability of the intercalated clay complex.

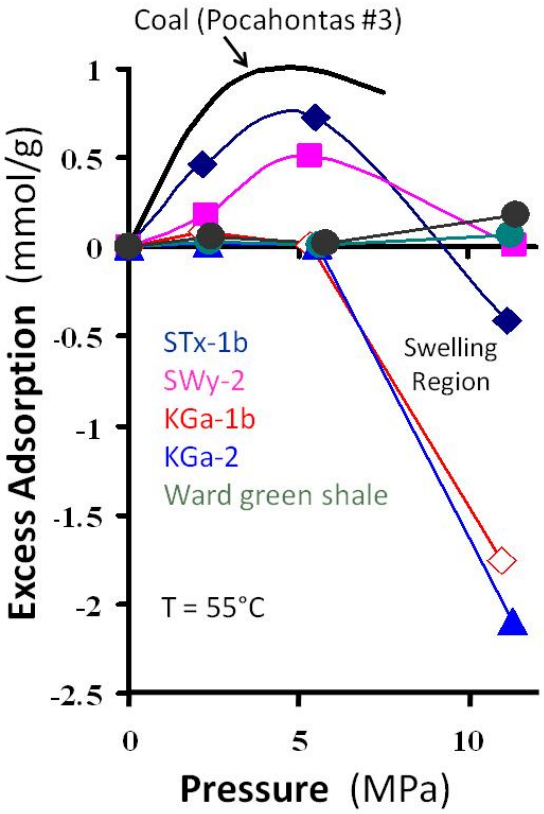

Figure 1. Adsorption of CO_2 in coal and various clay materials; montmorillonite (STx) and kaolinite (KGa) samples exhibit limited adsorption at low pressures but swell at supercritical conditions above 10 MPa.

We have completed a series of molecular dynamics simulations to better assess the molecular interactions associated with incorporation of the CO_2 in the interlayer of montmorillonite, and to simulate vibrational spectra to help validate the models with experimental observation. This study follows the examples provided in previous efforts to link experimental vibrational analysis with large-scale molecular dynamics simulations of layered materials (Cygan et al., 2004; Ockwig et al., 2009). This computational chemistry investigation provides a proof of concept that molecular simulation methods have the capability and accuracy to predict the mechanisms associated with CO_2 capture in complex natural materials.

2. MOLECULAR SIMULATIONS

2.1. Molecular Models of Montmorillonite

Sodium montmorillonite is a common soil phase that results from the weathering and alteration of basic rock types typically having low potassium contents under alkaline conditions. The normally nano-sized platy material is characterized by planar sheets of silica tetrahedra and alumina octahedra that coordinate to form a TOT (tetrahedron-octahedron-tetrahedron) layer that is negatively charged by the aliovalent substitution of Mg^{+2} for Al^{3+} in the octahedral sheet (Figure 2). The negative charge is balanced by the incorporation of Na cations in the interlayer. Smectite clays, like montmorillonite, typically have a relatively low layer charge (c.f., muscovite) and therefore can be easily expanded by the insertion of water molecules into the interlayer to hydrate the Na^{+} and internal surface of the tetrahedral sheet. The general chemical formula for sodium montmorillonite is given by $Na_xMg_xAl_{2-x}Si_4O_{10}(OH)_2 \cdot nH_2O$ where all of the layer charge resides on the octahedral sheet, although tetrahedral substitutions such as Al^{3+} for Si^{4+} can also occur to augment the net negative layer charge. Hydroxyl groups in TOT clays are associated with the octahedra sheet. Montmorillonite has hydroxyl groups that are affected by vacancies that occur for every two occupied Al octahedra (see Figure 2). Silica tetrahedra form a hexagonal ring structure (as viewed along the *c*-axis) that influences the disposition of interlayer species. Figure 2 shows interlayer Na^{+} that binds at the hexagonal holes in the tetrahedral sheet, which in turn modifies the equilibrium position of the hydroxyl groups directly above the hole.

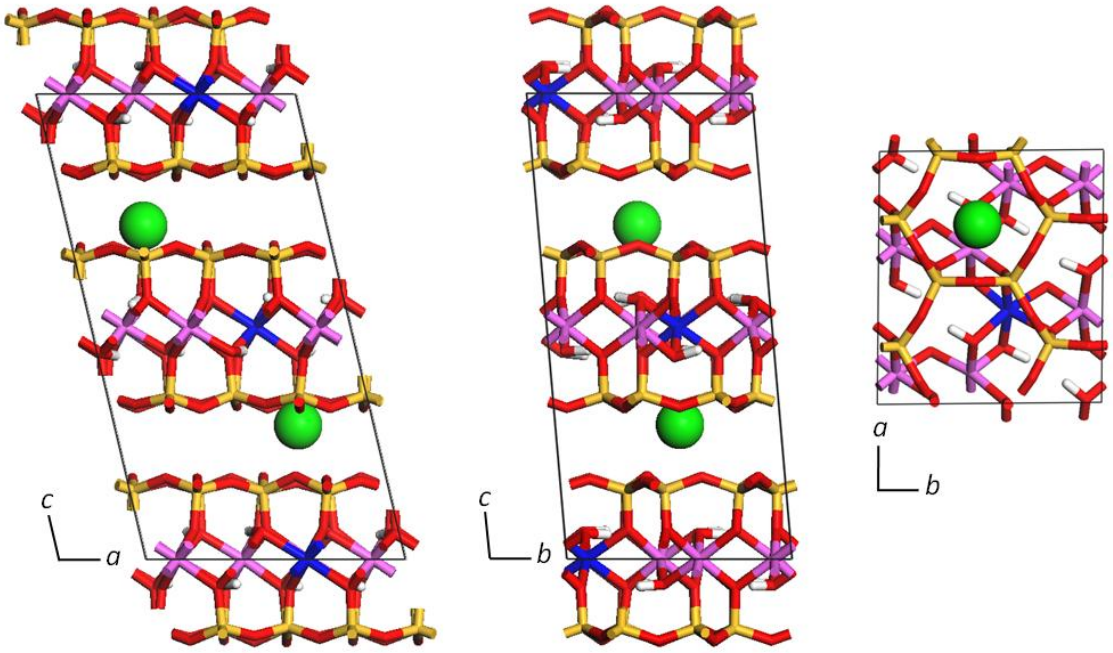

Figure 2. Structure of 2 x 1 x 2 Na-montmorillonite cell exhibiting two layers of the aluminosilicate lattice; Mg atoms (blue) substitute for Al (pink) in the octahedral sheet; interlayer Na cations are represented as green spheres.

An expanded representation of sodium montmorillonite is presented in Figure 3 where the clay is based on the smaller structure of Figure 2 with the addition of a single layer of water in the interlayer. The equilibrated structure is taken from a large-scale molecular dynamics simulation a 6 x 4 x 2 supercell having 36 Na^+ and 192 water molecules in the interlayer. Details of the molecular dynamics simulations are discussed in Section 2.2.1.

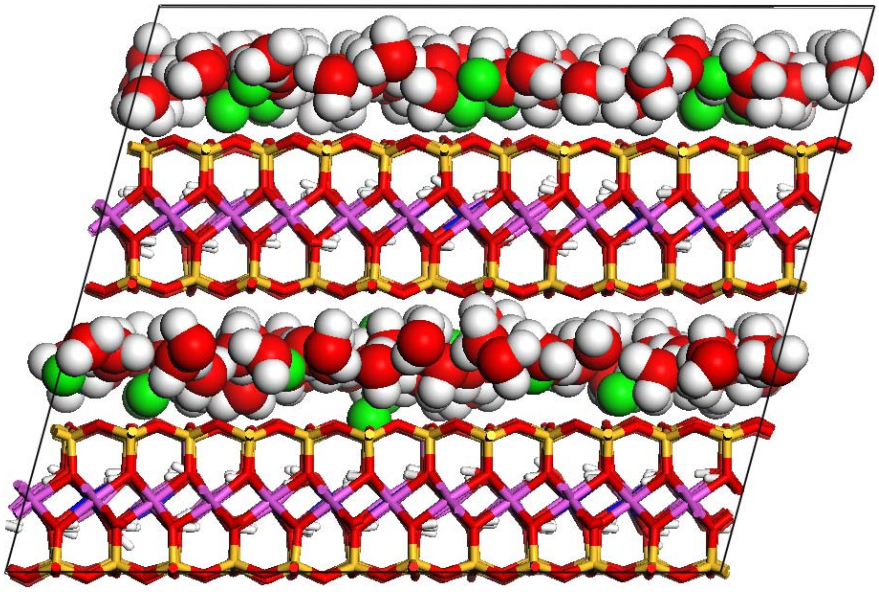

Figure 3. Snapshot of an equilibrated molecular dynamics simulation of sodium montmorillonite showing the Na^+ and water molecules in the interlayer; projection view is along the *b*-axis.

Because of the nano-sized nature of clay materials and lack of suitable large single crystals for accurate structure determinations, molecular simulations have played a significant role in understanding clay structure and behavior. The swelling behavior of clay phases, in particular, has been examined to better evaluate the energy and hydration state of clay minerals (e.g., Cygan et al., 2004; Smith et al., 2006). Figure 4 presents the results of a series of molecular dynamics simulations using an isothermal-isobaric ensemble to evaluate the expansion of the clay with increasing water content. This example, from Cygan et al. (2004), shows the expansion of montmorillonite with the development of a hydrogen bonded network of water molecules and the solvation of Na^+ to stabilize the interlayer and overcome the electrostatics that holds the layers together. Once expanded, the open interlayer region allows the backfill of water molecules to further stabilize the hydrogen bonding network until a critical water content is reached and the clay interlayer swells to accommodate two water layers. The fine structure of the swelling curve is in very good agreement with experimental findings (Fu et al., 1990). The simulations also suggest the possibility of forming a third water layer that becomes somewhat diffuse at the higher water content, but which is not observed in experiment.

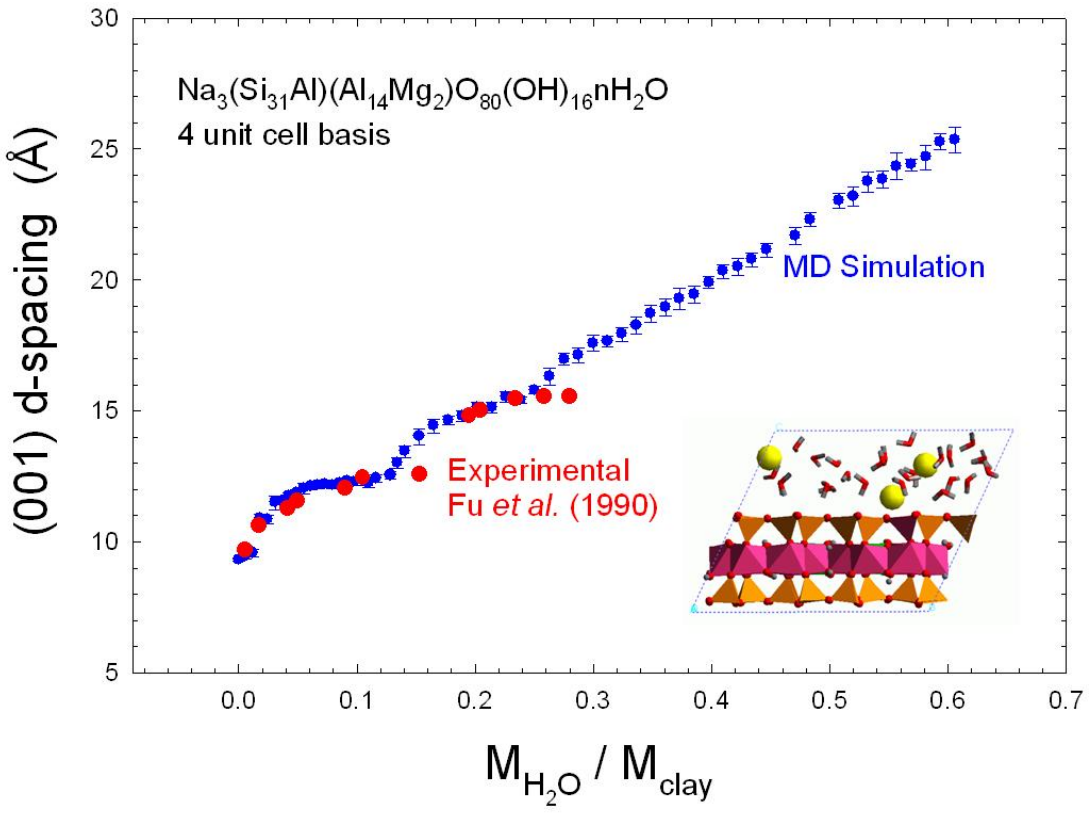

Figure 4. Swelling behavior of a montmorillonite clay based on *NPT* molecular dynamics simulations.

2.2. Computational Methods

2.2.1. Classical Methods

Classical molecular dynamics (MD) was used to evaluate the structure and behavior of gaseous, liquid, and supercritical CO_2, montmorillonite, and CO_2-intercalated montmorillonite. Quantum chemistry methods, including those based on density functional theory, are theoretically more accurate but computationally expensive and cannot efficiently simulate the large number of atoms and time steps necessary to accurately model clay structures. We employ the Clayff force field (Cygan et al., 2004) that uses an empirically-derived set of interaction parameters to accurately describe the potential energy between atoms in the clay structure. Clayff has been used extensively to successfully simulate many oxide, hydroxide, and hydrated systems including bulk and interfacial structures (see Cygan et al., 2004). The Forcite software (Accelrys, 2009) and Clayff parameters were used to evaluate the electrostatic and short-range interactions for each atomic configuration and time step.

Unfortunately, empirical force fields for the accurate simulation of CO_2 systems have not been fully developed, especially for interactions with oxide and silicate materials. Three-site models for CO_2 that are most compatible with Clayff have been examined (e.g., Harris and Yung, 1995;

Qin et al., 2008), but the models lack bond flexibility and are incapable of providing an accurate description of the vibrational behavior of gaseous and condensed carbon dioxide liquids. A fully flexible model is required in order to evaluate the vibrational state of carbon dioxide within the clay interlayer, especially if vibrational spectroscopy is to provide an accurate diagnostic tool for CO_2 intercalation. Details of the force field development are provided in Section 3.1.1.

Molecular dynamics simulations were performed using either a canonical *NVT* ensemble maintaining a fixed cell volume for a fixed number of atoms, or an isothermal-isobaric *NPT* ensemble where the simulations cell can freely expand or contract. All simulation cells have *P*1 symmetry where all atoms are allowed to freely translate throughout the entire simulation. Temperature was controlled using the Nosé-Hoover (1984) method, and the Berendsen et al. (1984) algorithm was used for controlling pressure of the simulation cell. One million time steps of 1 fs were used for most of CO_2 simulations to obtain a total of 1 ns of simulation time; atomic configurations were saved every 1000 time steps (1 ps) for efficient data storage and trajectory analysis. MD simulations were performed at various temperatures and pressures for evaluating subcritical CO_2, and at 310 K (constant volume) or 310 K and 0.02 GPa for the *NPT* ensemble for supercritical CO_2 simulations. MD simulations for montmorillonite and CO_2-montmorillonite systems were completed at 300 K and 0.0001 GPa or 310 K and 0.02 GPa, using 1 fs time steps for 1 ns of total simulation time. Once equilibrated, an additional 40 ps of simulation was performed for each system saving atomic positions and velocities for power spectra determinations. Simulations of gas phase CO_2 used periodic cells including 176 to1408 molecules whereas calculations of liquid and supercritical CO_2 used 512 molecules. Clay-CO_2 simulations involved a 6 x 4 x 2 supercell of montmorillonite having 40 CO_2 molecules corresponding to a density equivalent to that of liquid CO_2.

Power spectra are derived from the stored atomic velocities by evaluating the velocity autocorrelation function (VACF) and the Fourier-transformed power spectra (Allen and Tildesley, 1987). For power spectra calculations, the atomic velocities were collected every 4 fs over a simulation time of 40 ps. Sampling every 4 fs ensured that the vibrational modes up to 4166 cm^{-1} were captured. A windowing gap of 1,500 frames (6 ps) was used to give a resolution of approximately 2.8 cm^{-1}. The resulting power spectra represent the coordinated motions of atoms that correlate to bond stretches, bond angle bends, librations, intermolecular motions, and translations. Typically, the power spectrum modes are equivalent to the vibrational bands associated with infrared and Raman spectra but without the limitations of selections rules.

2.2.2. Quantum Methods

High-level electronic structure calculations and normal mode analysis were performed for cluster models of CO_2 and Na^+-CO_2. The Gaussian software was used to examine the clusters at two levels of theory. A hybrid functional B3LYP was implemented that combines the Becke (1993) hybrid functional for Hartree-Fock exchange and DFT correlation with the local correlation of Vosko et al. (1980) and the nonlocal correlation of Lee et al. (1988). The Møller-Plesset (1934) correction for the correlation energy in a Hartree-Fock calculation, truncated at the second order (MP2), was used to investigate the two cluster models (Frisch et al., 1990a, 1990b). Aug-cc-pVDZ basis set was used for each of the two methods. Vibrational analysis of the optimized

structures was then performed to derive the normal modes of the clusters (Foresman and Frisch, 1996).

3. RESULTS AND DISCUSSION

3.1. Classical Simulations

3.1.1. Development of CO_2 Force Field

A general review of the computational chemistry literature determined that energy force fields for the classical simulation of CO_2 systems were limited, especially for a force field based on a three-site model of CO_2. Our primary goal for the project was to use a simple three-site model that could easily be coupled with similar preexisting force fields that accurately model water, aqueous solutions, and mineral systems. Furthermore, we desired a fully flexible force field that would allow the direct coupling of energy and momentum between liquids and solids for accurate interfacial simulations. Correct models of surface structures, transport rates, electrostatics, electric double layers, and other critical phenomena require full relaxation of the molecular system without any atomic constraints such as keeping part of the system rigid. It is also important for molecules like H_2O and CO_2 to include bond stretch and bond bend terms in the force field to provide vibrational data, help to characterize interfacial behavior, and support experimental and spectroscopic analyses.

Rigid models for CO_2 are common and have been successfully developed to accurately model the structure and thermodynamics of gas, liquid, and supercritical CO_2 (e.g., Murthy et al., 1981; Harris and Yung, 1995; Zhang and Duan, 2005; Nieto-Draghi et al., 2007). The Harris and Young (1995) potential model, in particular, is very successful in reproducing the vapor-liquid coexistence curve for CO_2 and has been modified to include a flexible bond angle. The van der Waals potential and the point charges were optimized to reproduce the correct pressures, internal energies, and quadrupole moment. However, the force constant for the bond angle term was not fully developed and fails to predict the experimental deformation mode for vibration of the molecule. Nieto-Draghi et al. (2007) used quantum mechanical calculations to evaluate bond stretch energies and a force constant for determination of thermal conductivity and shear viscosity of CO_2 but did not evaluate vibrational behavior. Qin et al. (2008) used the Harris and Young (1995) potential, adding a bond stretch term, to evaluate supercritical CO_2 and its interactions on silica surfaces. However, no critical examination was made on the choice of force constants and their effect on vibrational spectra or interfacial structure.

In our molecular simulations, we expand the previous three-site potentials for CO_2 and develop a fully flexible model, allowing for intramolecular bond stretch and angle bend. Equation (1) provides the general expression of the total potential energy in terms of the contributing terms.

$$E_{\text{Total}} = E_{\text{Coul}} + E_{\text{VDW}} + E_{\text{Stretch}} + E_{\text{Bend}} \quad (1)$$

Coulombic and van der Waals contributions represent the nonbonded energies and the stretch and bend terms represent the intramolecular energies. The Coulombic or electrostatics energy is given by equation (2) where q_i and q_j are the partial charges of the atoms and r_{ij} is the distance between the atoms.

$$E_{\mathrm{Coul}} = \frac{q_i q_j}{r_{ij}} \tag{2}$$

We assume electrostatics interactions occur in vacuum and that no dielectric medium is present to limit the interaction. A conversion factor is used to maintain appropriate energy units (kJ/mol) for this equation. The short-range van der Waals energy is given by:

$$E_{\mathrm{VDW}} = 4\varepsilon_{ij}\left[\left(\frac{\sigma_{ij}}{r_{ij}}\right)^{12} - \left(\frac{\sigma_{ij}}{r_{ij}}\right)^{6}\right] \tag{3}$$

where ε_{ij} and σ_{ij} are optimized for intermolecular interactions. Standard mixing rules are used to evaluate heteroatomic interactions for this expression (Halgren, 1992). Harmonic potentials are used for the bond stretch and angle bend terms:

$$E_{\mathrm{Stretch}} = \frac{1}{2}k_{\mathrm{S}}\left(r_{ij} - r_o\right)^2 \tag{4}$$

$$E_{\mathrm{Bend}} = \frac{1}{2}k_{\mathrm{B}}\left(\theta_{ijk} - \theta_o\right)^2 \tag{5}$$

Both energy expressions increase the potential energy using force constants k_S and k_B and deviations from the equilibrium geometry (r_o and θ_o). The total potential energy for any configuration of CO_2 molecules in a periodic simulation cell is evaluated using this set of potentials by summing all possible pair-wise interactions. Ewald summation is used to ensure convergence of the long-range Coulombic energy (equation 2). The Coulombic and van der Waals contributions are excluded when evaluating intramolecular interactions.

Our refinement of force field parameters was obtained by combining the expanded potentials of Zhu et al. (2009) based on the original parameters of Harris and Yung (1995). We initially incorporated the force constants of Qin et al. (2008) and Liang and Lipscomb (1990) but were disappointed in their poor performance in simulating vibrational spectra for CO_2 phases. Ultimately, we optimized the stretch and bend force constants through a series of molecular dynamics simulations and power spectra calculations. The force constant for the CO_2 bend was determined by directly matching the observed frequency of 667 cm^{-1} (Günzler and Gremlich, 2002). The force constant for the bond stretch is more problematic due to the occurrence of symmetrical and asymmetrical modes, observed, respectively, at 1330 cm^{-1} and 2349 cm^{-1}; the symmetrical stretch mode is infrared inactive due to the lack of a net dipole during the vibrational motion. Because of the coupling of the two stretch modes through a single force constant, it was necessary to minimize the mismatch for the peaks while placing more weight on the asymmetric stretch that dominates the intensity in theoretical spectra. We incorporated the identical equilibrium bond distance and bend angle used by Zhu et al. (2009) for the intramolecular potentials for CO_2. The bend and asymmetrical peaks are in agreement with experiment to within 3 cm^{-1}, however, the frequency for the symmetrical stretch is under predicted by approximately 100 cm^{-1}. The nature of the potentials for the simple three-site model limits the decoupling of the stretch models and improving the accuracy of the symmetrical stretch frequency.

The optimized force field parameters for CO_2 are presented in Table 1. The parameters were used for the bulk CO_2 simulations and subsequently were combined with those in Clayff (Cygan et al., 2004) to model the intercalated CO_2 montmorillonite. As noted previously, we rely on the combination rules to evaluate the van der Waals interactions between the CO_2 and the clay surfaces.

Table 1. Force Field Parameters for CO_2

Nonbond		
q_C	+0.6512	e
q_O	-0.3256	e
ε_C	0.2340	kJ/mol
ε_O	0.6683	kJ/mol
σ_C	2.800	Å
σ_O	3.028	Å
Bond		
k_{CO}	8443	kJ/mol Å^2
$r_{o\,CO}$	1.162	Å
k_{OCO}	451.9	kJ/mol rad^2
$\theta_{o\,OCO}$	180.0	°

3.1.2. Molecular Dynamics Simulations

Results from the molecular dynamics simulations of the CO_2 simulations using the updated force field are, in general, consistent with the thermodynamics and structures of Zhu et al. (2009). We observer no significant difference in the results with the modification of the intramolecular force constants and equilibrium bond length and bond angle. Equilibrium structures from the bulk supercritical CO_2 simulations (310 K and 0.020 GPa) indicate a bond angle distribution with a mean value of 178° that varies from the linear geometry obtained by Vorholz et al. (2000) for simulations at ambient conditions. The bond bend deformation leads to a net dipole moment for CO_2 at supercritical conditions and which may control the various dimer geometries that have been predicted and observed (Cabaço et al., 2008).

Figure 5 provides snapshots of the equilibrated simulation cells from the molecular dynamics calculations of gas and liquid CO_2. Resulting densities are consistent with the equilibrium coexistence curves for both phases at 300 K as reported by National Institute of Standards and Technology. A snapshot of the equilibrated CO_2-montmorillonite structure shows the distribution of a monolayer of CO_2 molecules arranged along the *ab*-plane of the clay interlayer (Figure 6). The mean basal *d*-spacing for the CO_2-intercalated clay is 12.23 Å which is smaller and almost indistinguishable from the 12.35 Å spacing observed for an equivalent hydrated clay. We observe on average about four CO_2 molecules coordinated to each of the interlayer sodium ions.

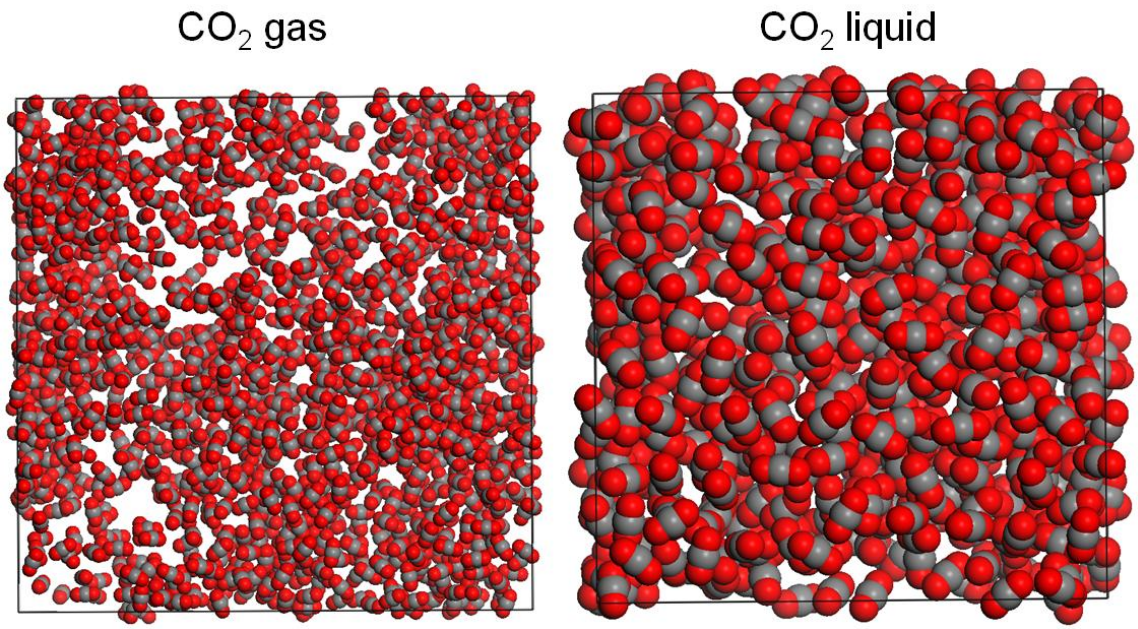

Figure 5. Simulation cells for molecular dynamics simulations of CO_2 as gas with 1408 molecules (left) and liquid with 512 molecules (right). Both simulations were equilibrated at 300 K and 5.6 MPa.

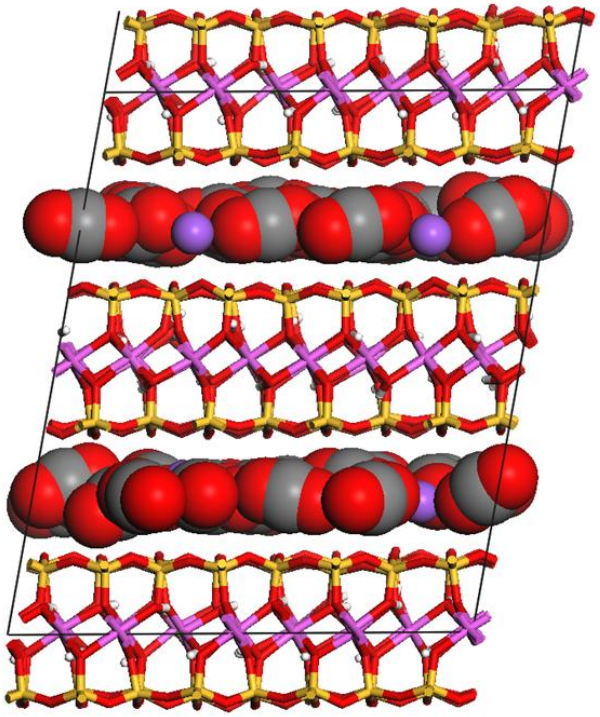

Figure 6. Equilibrated supercell structure of CO_2-montmorillonite model from molecular dynamics simulation using *NPT* ensemble at 310 K and 0.02 GPa. Projection view is along *b*-axis.

3.1.3. Power Spectra

Power spectra derived from the molecular dynamics trajectories for the gas and liquid CO_2 simulations are presented in Figure 7. Carbon dioxide, a linear molecule, is expected to have $3N - 5$ (N is number of atoms) or four vibrational modes. The bending mode is doubly degenerate so only three peaks are observed in the power spectra. The vibrational frequencies are nearly identical for the two phases and only the intensity varies between the simulations. The asymmetrical stretch mode is the most intense vibrational mode for the liquid while the bend mode dominates the gas. The results overall are consistent with observation. The low frequencies at less than 100 cm^{-1} represent molecular translations—diffusion of CO_2 molecules in the simulation cell during the 6 ps window used to evaluate the correlated atomic velocities. The greater intensity observed for the gas phase relative to the liquid is consistent with molecular diffusion and the different densities of the two simulation cells. The low frequency region between 100 and 200 cm^{-1} is associated with intermolecular associations of CO_2.

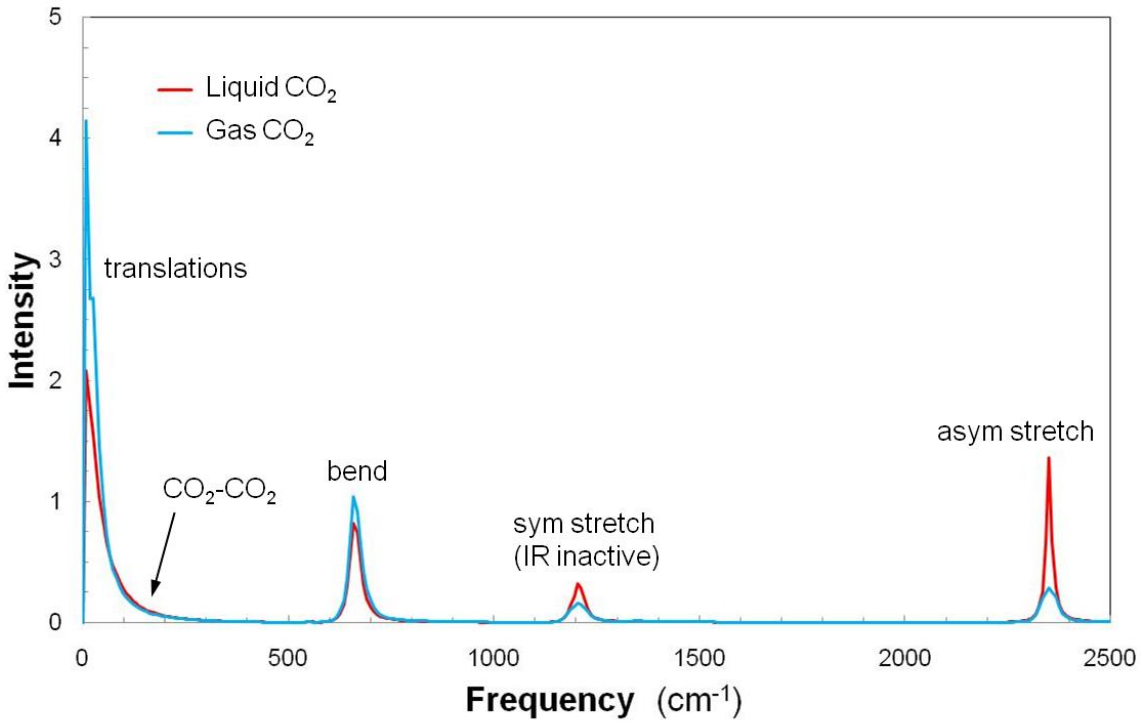

Figure 7. Power spectra for gas and liquid forms of CO_2 at 300 K and 5.6 MPa.

Figure 8 provides the power spectrum for the equilibrated CO_2-montmorillonite based on the velocity autocorrelation for all atoms in the simulation. The hydroxyl stretch dominates the spectrum at the highest frequencies and is associated with the hydroxyls coordinated to the octahedral aluminum in the montmorillonite layer. The bend mode and two stretch modes for CO_2 are also observed at the same frequencies noted previously. The most intense peak is for the CO_2 asymmetric stretch as observed in simulations of liquid CO_2. Spectral features at the lower

frequencies are dominated by metal-oxygen stretch and various oxygen-metal-oxygen bends from tetrahedral silicon and octahedral aluminum. Intermolecular CO_2 interactions probably contribute to some of the intensity along the tail of the translations peak at 100 to 200 cm^{-1}.

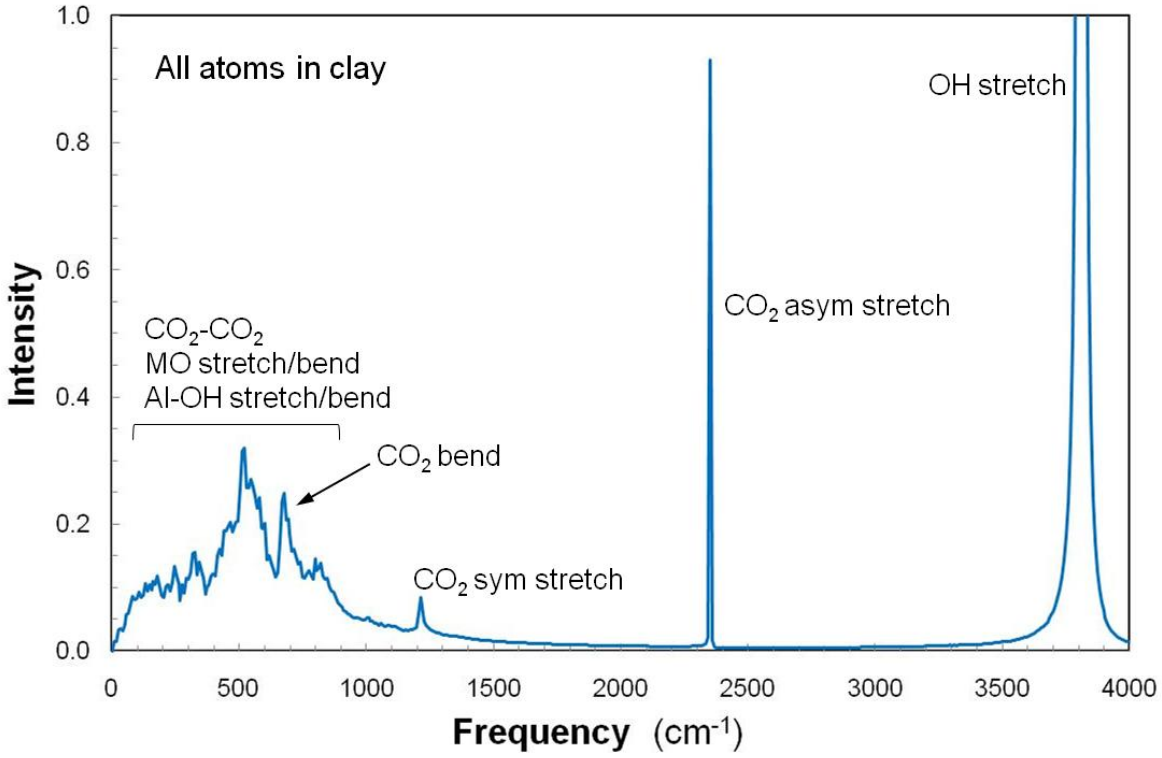

Figure 8. Power spectrum for the CO_2-montmorillonite derived from analysis of all atoms in the molecular dynamics trajectory.

The benefit of using molecular simulations and power spectrum analysis is the ability to separate complex signals and identify specific contributors to the spectrum. This process is best demonstrated in our VACF analysis using only the interlayer CO_2 atoms and removing the clay atoms from the analysis. The Fourier transform of the VACF for the CO_2 component from the CO_2-montmorillonite simulation is presented in Figure 9 along with the power spectrum obtained from the liquid CO_2 simulation as a reference. The power spectrum for the intercalated CO_2, in general, is similar to that for the liquid. The relative intensities are consistent although the asymmetrical stretch mode for the intercalated CO_2 exhibits enhanced intensity, along with a narrowing of the peak, associated with the confinement of the interlayer and direct interaction with two silicate surfaces. The enhanced intensity is probably due to additional induced dipole-ion interactions. The symmetrical stretch for CO_2 occurs at 1210 cm^{-1} with a slight narrowing and subtle shift to higher frequencies. However, the bend mode for CO_2 at 667 cm^{-1} is significantly shifted (approximately 10 to 15 cm^{-1}) to higher frequencies (Figure 10) with intercalation into the montmorillonite. Although it is not clear whether the shift is controlled by the confining space of the interlayer or the association of CO_2 with the interlayer Na^+, the

predicted peak shift appears to be diagnostic of intercalated CO_2. Lastly, the broad peak at low frequency, attributed to intermolecular CO_2 interactions, is greatly amplified relative to those librations for liquid CO_2.

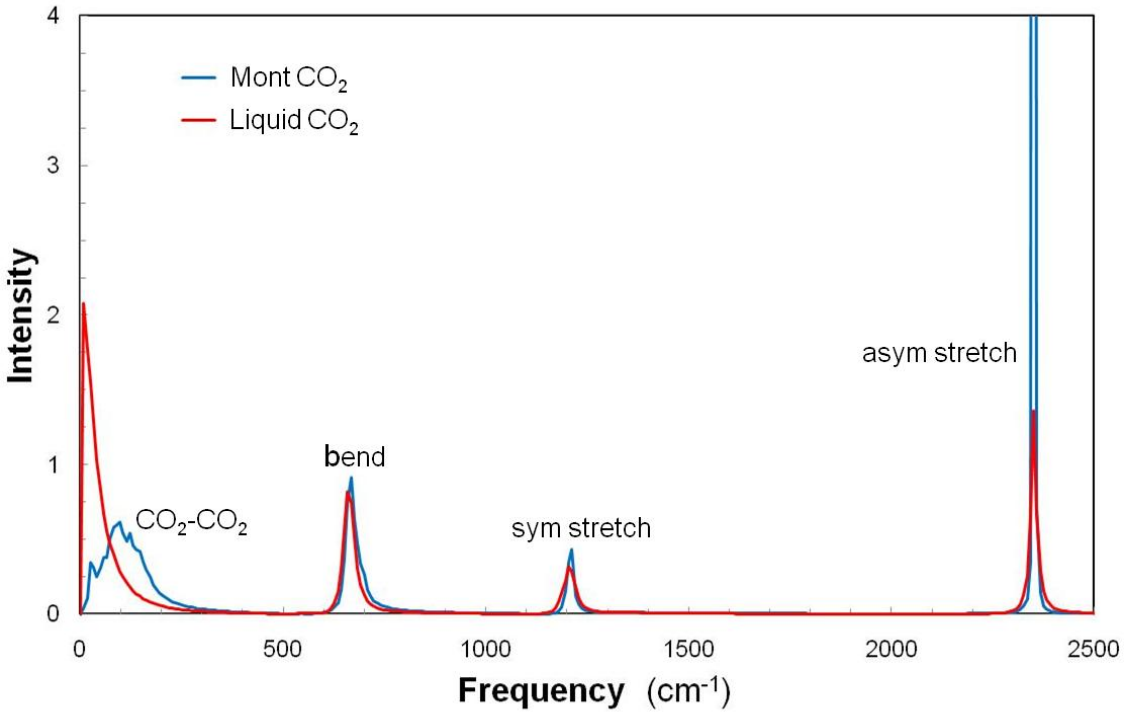

Figure 9. Power spectra for the CO_2 atoms in liquid CO_2 and interlayer CO_2 from the intercalated montmorillonite derived from analysis of the molecular dynamics trajectories.

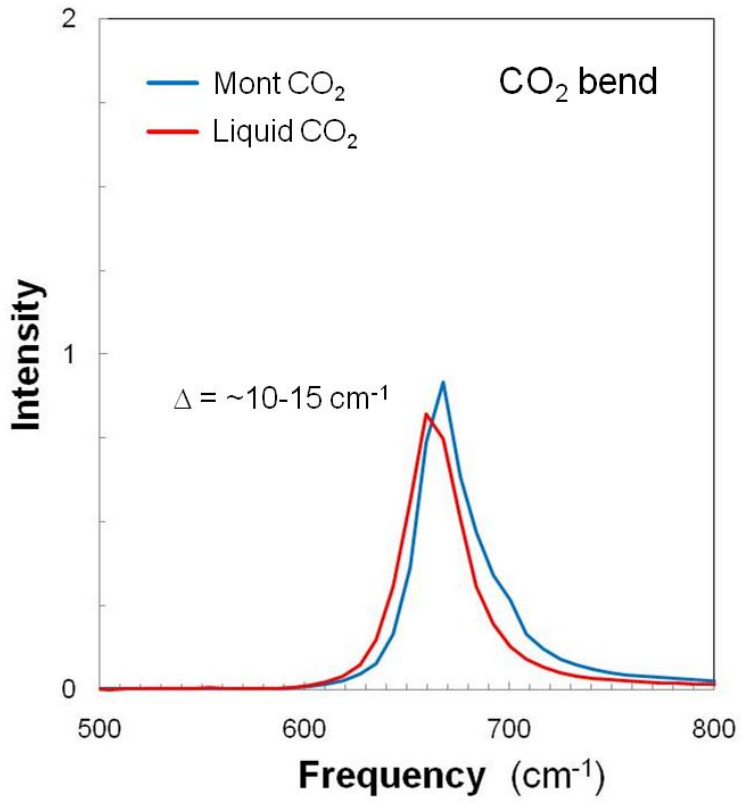

Figure 10. Detail of the CO_2 bend mode in the power spectra for the CO_2 atoms in liquid CO_2 and interlayer CO_2 from the intercalated montmorillonite.

3.2. Quantum Simulations

We used electronic structure calculations to derive optimized configurations of isolated CO_2 and Na^+-CO_2 clusters. Optimized structures using the Gaussian03 software package were obtained at the B3LYP/Aug-cc-pVDZ and MP2/Aug-cc-pVDZ levels of theory and subsequently used for normal mode analysis to derive vibrational intensities and frequencies. A linear configuration of the CO_2 molecule with Na^+ is observed for the optimized structures using both methods. The electrostatics control the strong interaction of the cation with either of the terminal oxygen atoms. The normal mode results for the optimized clusters (Table 2) indicate a shift to lower frequencies for all modes using the MP2 methods relative to those obtained using the B3LYP functionals. In both methods, we observe a blue shift of about 40 cm^{-1} in the asymmetrical stretch frequency of CO_2 to approximately 2420 cm^{-1} when the molecule is associated with Na^+. Similarly, there is a blue shift of approximately 15 cm^{-1} for the symmetrical stretch. In contrast, the experimental FT-IR spectrum of Na-montmorillonite with intercalated CO_2 suggests a small red shift (5 cm^{-1}) of the asymmetric CO_2 stretch. This different observation suggests that the confinement environment of the clay phase could be responsible for the peak shift. The MD simulations of the Na-montmorillonite-CO_2 system predict virtually no dependency of the asymmetric stretch mode upon intercalation, somewhat comparable to the experimental observation. In this regard, the blue shift of the bending mode of CO_2 predicted using the MD

simulations can also be associated with the confinement environment of the interlayer region. We observe in the cluster calculations that the interaction with Na^+ alone leads to the opposite trend.

Table 2. Normal Mode Analysis of Quantum-Derived CO_2 Cluster Models

	O=C=O			Na^+...O=C=O		
Method	**Symmetry**	**IR Intensity**	**Frequency**	**Symmetry**	**IR Intensity**	**Frequency**
			cm^{-1}			cm^{-1}
B3LYP/ Aug-cc-pVDZ	Sg	656.54	2388.58	Sg	696.94	2423.42
	Sg	0	1354.38	Sg	25.83	1367.75
	Pi	28.75	667.52	Pi	33.81	653.05
	Pi	28.75	667.52	Pi	33.81	653.05
				Sg	43.47	220.65
				Pi	7.44	76.19
				Pi	7.44	76.19
MP2/ Aug-cc-pVDZ	Sg	567.61	2379.38	Sg	428.55	2420.59
	Sg	0	1305.47	Sg	14.14	1320.70
	Pi	21.46	655.45	Pi	26.14	641.97
	Pi	21.46	655.45	Pi	26.14	641.97
				Sg	68.85	204.35
				Pi	7.76	65.16
				Pi	7.76	65.16

4. CONCLUSIONS

We have completed a series of molecular dynamics simulations to better assess the molecular interactions associated with incorporation of CO_2 in the interlayer of montmorillonite clay, and to simulate vibrational spectra to help validate the models with experimental observation. We first extended several published three-site potential models of CO_2 to derive a set of accurate interaction parameters that are compatible with the widely-used Clayff force field. The extended set of interaction parameters permits full flexibility of the molecule allowing bond stretching and bond angle bending. Comparison of experimental and theoretical data with our molecular dynamics simulations of gas and liquid CO_2 confirms the accuracy of the new force field. Based on the experimental evidence for CO_2 intercalation in montmorillonite clay, we developed a conceptual model for the intercalated structure and performed a series of molecular dynamics simulations. Power spectra were derived from the equilibrated atomic and velocity trajectories that allowed the isolation of signal from key components of the molecular model. Normal model analysis of optimized structures of CO_2 and Na-CO_2 derived from density functional calculations are in general agreement with the classical models although the trends in vibrational frequencies are inconsistent with experiment and MD simulations of Na^+-montmorillonite-CO_2 system suggesting that the confinement environment plays a dominant role in the direction of those frequency shifts. Power spectra analyses of the molecular dynamics trajectories indicate the bending motion of CO_2 at approximately 667 cm^{-1} is blue shifted by 10 to 15 cm^{-1} when CO_2 is in the clay interlayer. The asymmetric stretch of CO_2 at 2349 cm^{-1} is virtually unaffected by the environment of the clay interlayer and occurs at the same frequency as that for liquid CO_2. This result is similar to experimental findings from diffuse reflectance infrared spectroscopy showing that the asymmetrical stretch mode is red-shifted only slightly (10 cm^{-1} in Ca-montmorillonite and 5 cm^{-1} in Na-montmorillonite) upon intercalation. This computational chemistry investigation provides a proof of concept that molecular simulation methods can provide important insights into the possible molecular mechanisms associated with CO_2 capture in complex natural materials.

5. REFERENCES

Accelrys. (2009) Materials Studio Software. Accelrys, Inc., San Diego.

Allen, M.P. and Tildesley, D.J. (1987) *Computer Simulation of Liquids*. 385 p. Oxford University Press, Oxford.

Bacsik, Z., Atluri, R., Garcia-Bennett, A.E., and Hedin, N. (2010) Temperature-induced uptake of CO_2 and formation of carbamates in mesocaged silica modified with n-propylamines. *Langmuir*, 26(12), 10013-10024.

Becke, A.D. (1993) Density functional thermochemistry: 3. The role of exact exchange. *Journal of Chemical Physics*, 98(7), 5648-5652.

Berendsen, H.J.C., Postma, J.P.M., Vangunsteren, W.F., Dinola, A., and Haak, J.R. (1984) Molecular dynamics with coupling to an external bath. *Journal of Chemical Physics*, 81(8), 3684-3690.

Cabaço, M.I., Longelin, S., Danten, Y., and Besnard, M. (2008) Transient dimer formation in supercritical carbon dioxide as seen from Raman scattering. *Journal of Chemical Physics*, 128(7), 074507.

Cygan, R.T., Liang, J.-J., and Kalinichev, A.G. (2004) Molecular models of hydroxide, oxyhydroxide, and clay phases and the development of a general force field. *Journal of Physical Chemistry B*, 108(4), 1255-1266.

Favre, E., Bounaceur, R., and Roizard, D. (2009) Biogas, membranes and carbon dioxide capture. *Journal of Membrane Science*, 328(1-2), 11-14.

Foresman, J.B. and Frisch, A. (1996) *Exploring Chemistry with Electronic Structure Methods: A Guide to Using Gaussian*. Gaussian, Inc., Pittsburgh.

Frisch, M.J., Headgordon, M., and Pople, J.A. (1990a) A direct MP2 gradient method. *Chemical Physics Letters*, 166(3), 275-280.

Frisch, M.J., Headgordon, M., and Pople, J.A. (1990b) Semidirect algorithm for the MP2 energy and gradient. *Chemical Physics Letters*, 166(3), 281-289.

Fu, M.H., Zhang, Z.Z., and Low, P.F. (1990) Changes in the properties of a montmorillonite-water system during the adsorption and desorption of water: Hysteresis. *Clays and Clay Minerals*, 38(5), 485-492.

Günzler, H. and Gremlich, H. (2002) *IR Spectroscopy: An Introduction*. Wiley-VCH, New York.

Halgren, T.A. (1992) Representation of van der Waals (vdW) interactions in molecular mechanics force fields: Potential form, combination rules, and vdw parameters. *Journal of the American Chemical Society*, 114(20), 7827-7843.

Harris, J.G. and Yung, K.H. (1995) Carbon dioxide's liquid-vapor coexistence curve and critical properties as predicted by a simple molecular model. *Journal of Physical Chemistry*, 99(31), 12021-12024.

Lee, C.T., Yang, W.T., and Parr, R.G. (1988) Development of the Colle-Salvetti correlation energy formula into a fucntional of the electron density. *Physical Review B*, 37(2), 785-789.

Liang, J.Y. and Lipscomb, W.N. (1990) Binding of substrate CO_2 to the active site of human carbonic anhdrase II: A molecular dynamics study. *Proceedings of the National Academy of Sciences of the United States of America*, 87(10), 3675-3679.

Møller, C. and Plesset, M.S. (1934) Note on an approximation treatment for many-electron systems. *Physical Review*, 46(7), 618-622.

Murthy, C.S., Singer, K., and McDonald, I.R. (1981) Interaction site models for carbon dioxide. *Molecular Physics*, 44(1), 135-143.

Nieto-Draghi, C., de Bruin, T., Perez-Pellitero, J., Avalos, J.B., and Mackie, A.D. (2007) Thermodynamic and transport properties of carbon dioxide from molecular simulation. *Journal of Chemical Physics*, 126(6), 064509.

Nosé, S. (1984) A molecular dynamics method for simulations in the canonical ensemble. *Molecular Physics*, 52(2), 255-268.

Ockwig, N.W., Greathouse, J.A., Durkin, J.S., Cygan, R.T., Daemen, L.L., and Nenoff, T.M. (2009) Nanoconfined water in magnesium-rich 2:1 phyllosilicates. *Journal of the American Chemical Society*, 131(23), 8155-8162.

Qin, Y., Yang, X.N., Zhu, Y.F., and Ping, J.L. (2008) Molecular dynamics simulation of interaction between supercritical CO_2 fluid and modified silica surfaces. *Journal of Physical Chemistry C*, 112(33), 12815-12824.

Smith, D.E., Wang, Y., Chaturvedi, A., and Whitley, H.D. (2006) Molecular simulations of the pressure, temperature, and chemical potential dependencies of clay swelling. *Journal of Physical and Chemical B*, in press.

Vorholz, J., Harismiadis, V.I., Rumpf, B., Panagiotopoulos, A.Z., and Maurer, G. (2000) Vapor plus liquid equilibrium of water, carbon dioxide, and the binary system, water plus carbon dioxide, from molecular simulation. *Fluid Phase Equilibria*, 170(2), 203-234.

Vosko, S.H., Wilk, L., and Nusair, M. (1980) Accurate spin-dependent electron liquid correlation energies for local spin density calculations: A critical analysis. *Canadian Journal of Physics*, 58(8), 1200-1211.

Wang, L., Zhang, M., and Redfern, S.A.T. (2003a) Infrared study of CO_2 incorporation into pyrophyllite $Al_2Si_4O_{10}(OH)_2$ during dehydroxylation. *Clays and Clay Minerals*, 51(4), 439-444.

Wang, Y., Bryan, C., Xu, H., and Gao, H. (2003b) Nanogeochemistry: Geochemical reactions and mass transfer in nanopores. *Geology*, 31(5), 387-390.

Zhang, Z.G. and Duan, Z.H. (2005) An optimized molecular potential for carbon dioxide. *Journal of Chemical Physics*, 122(21), 214507.

Zhao, G.Y., Aziz, B., and Hedin, N. (2010) Carbon dioxide adsorption on mesoporous silica surfaces containing amine-like motifs. *Applied Energy*, 87(9), 2907-2913.

Zhu, A.M., Zhang, X.B., Liu, Q.L., and Zhang, Q.G. (2009) A fully flexible potential model for carbon dioxide. *Chinese Journal of Chemical Engineering*, 17(2), 268-272.

DISTRIBUTION

1 Stephen Guggenheim
Department of Earth and Environmental Sciences
University of Illinois at Chicago
Chicago, IL 60607-7059

1 George D. Guthrie
Geological and Environmental Systems
National Energy Technology Laboratory
P.O. Box 10940
Pittsburgh, PA 87545

1 August F. Koster van Groos
Department of Earth and Environmental Sciences
University of Illinois at Chicago
Chicago, IL 60607-7059

2 Evgeniy M. Myshakin
URS
National Energy Technology Laboratory
P.O. Box 10940
Pittsburgh, PA 15236

2 Vyacheslav N. Romanov
Geosciences Division
National Energy Technology Laboratory
P.O. Box 10940
Pittsburgh, PA 15236

1	MS 0735	J. A. Merson	6910
1	MS 0754	S. J. Altman	6915
1	MS 0754	L. J. Criscenti	6915
10	MS 0754	R. T. Cygan	6915
1	MS 0754	M. J. Rigali	6915
1	MS 0895	S. B. Rempe	8635
1	MS 1415	K. Leung	1114

1	MS 0359	D. L. Chavez, LDRD Office	1911
1	MS 0899	Technical Library	9536 (electronic copy)


Sandia National Laboratories